View metadata, citation and similar papers at core.ac.uk

brought to you by CORE

provided by IntechOpen

We are IntechOpen, the world's leading publisher of Open Access books Built by scientists, for scientists

4,800
Open access books available

122,000
International authors and editors

135M
Downloads

Our authors are among the

154
Countries delivered to

TOP 1%
most cited scientists

12.2%
Contributors from top 500 universities

CLARIVATE ANALYTICS BOOK CITATION INDEX INDEXED

WEB OF SCIENCE™

Selection of our books indexed in the Book Citation Index in Web of Science™ Core Collection (BKCI)

Interested in publishing with us?
Contact book.department@intechopen.com

Numbers displayed above are based on latest data collected.
For more information visit www.intechopen.com

Chapter 2

Langmuir-Blodgett Methodology: A Versatile Technique to Build 2D Material Films

María Mercedes Velázquez, Teresa Alejo, David López-Díaz, Beatriz Martín-García and María Dolores Merchán

Additional information is available at the end of the chapter

http://dx.doi.org/10.5772/63495

Abstract

The Langmuir-Blodgett (LB) methodology is based on the transfer process of a monolayer adsorbed at the water interface, Langmuir film, from the air-water interface onto solids by vertical dipping of the substrate immersed on the subphase. The technique allows the continuous variation of material density, packing, and arrangement by compressing or expanding the film by using barriers. Consequently, it provides the possibility of preparing films with the control of interparticle distance necessary to exploit the two-dimensional (2D) materials in technological applications. In this chapter, we present some examples of fabrication of thin films of 2D material using this methodology. We show some methodologies based on this technique to build thin films of graphene oxides, Quantum Dots (QDs), and silver nanowires.

Keywords: Langmuir-Blodgett films, graphene oxide, silver nanowires, CdSe Quantum Dots, AFM, TEM, FESEM

1. Introduction

Dimensionality is one of the most fundamental material parameters because it defines the atomic structure of materials and determines its main properties. Thus, one chemical element or compound can exhibit different properties in different dimensions. Some interesting examples about size effect are surface plasmon resonance in metal nanoparticles, quantum confinement in semiconductor particles, and superparamagnetism in magnetic nanomaterials.

INTECH
open science | open minds

© 2016 The Author(s). Licensee InTech. This chapter is distributed under the terms of the Creative Commons Attribution License (http://creativecommons.org/licenses/by/3.0), which permits unrestricted use, distribution, and reproduction in any medium, provided the original work is properly cited. CC BY

If one dimension is restricted, we have two-dimensional (2D) or layered shape material. An interesting example of this kind of materials is graphene. This material is a monolayer of carbon atoms tightly packed into 2D honeycomb lattice that has attracted worldwide attention since it was discovered in 2004 [1, 2]. This new material has emerged with a promising future due to its amazing properties such as transparency, high-charge mobility, thermal conductivity, and mechanical resistance. Due to these unique properties, graphene has been proposed as a good candidate for manufacturing transparent-conducting electrodes, transistors, hydrogen-storage devices, and gas sensors [3, 4]. The growing interest on graphene has highlighted the importance of another 2D material in technological applications such as transition metal chalcogenides (TMC) and layered ionic solids.

Several 2D materials can be obtained by exfoliation of a layered bulk crystal. However, this procedure is often difficult because the van der Waals interactions between adjacent layers must be overcome. Mechanical exfoliation provides good results, but mostly applied for fundamental research because it is arduous and expensive to produce the material at industrial scale by this way. Other methodologies such as solvent-assisted ultrasound exfoliation [5] or chemical synthesis [6] allow obtaining large amounts of materials at low cost, although they present several disadvantages against mechanical exfoliation. One important disadvantage is related with the deposition of materials onto solids. Hence, for several technological applications, it is necessary to support 2D materials onto solid substrates [7, 8] and since the properties of 2D materials deposited onto solids are strongly affected by the film morphology, a deposition methodology becomes necessary, which allows a great control of the material density and packing. Several techniques such as drop casting [9] or spin coating [10] have been used to integrate these materials onto novel devices; however, they often lead to nonuniform films or films with aggregated materials due to uncontrolled capillary flow and dewetting processes during solvent evaporation. These aggregates decrease the specific properties of each material [2, 11]. An illustrative example of the aggregation produced by solvent evaporation can be seen in **Figure 1**. The figure shows a field emission scanning electron microscopy (FESEM) image of a graphene oxide (GO) film deposited onto silicon by drop casting.

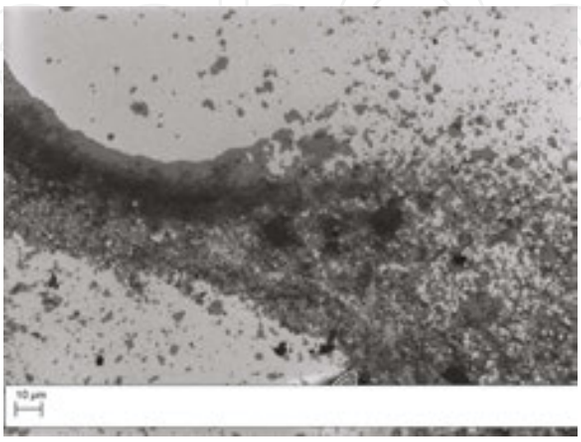

Figure 1. FESEM image of graphene oxide deposited onto silicon by drop casting.

http://dx.doi.org/10.5772/63495

An alternative technique is the Langmuir-Blodgett (LB) methodology. This method consists on the transfer process of a water-insoluble material from the air-water interface onto a solid substrate by vertical dipping of the solid in the Langmuir monolayer [12]. This technique allows continuous variation of material density, packing, and arrangement by compressing or expanding the film using barriers. Consequently, it offers the possibility of preparing films with the control of interparticle distance necessary to exploit the 2D materials in technological applications. Despite this methodology being successfully used for transferring water-insoluble molecules [12–14] and nanoparticles [15], it has been less employed to transfer graphene derivatives [16–19] or TMC materials onto solid substrates.

This chapter reviews some strategies to build 2D material films by means of the LB methodology. The content is organized into three main sections. The first one introduces the LB methodology. The second one summarizes the production of thin films of graphene oxide derivatives by using this methodology [17–20]. The last section describes some representative results concerning thin films of Quantum Dots (QDs) of transition metal chalcogenides [21–26] and silver nanowires (AgNWs) [27]. All sections are focused on the possibility of tuning the morphology of the 2D material by modifying the surface composition of the Langmuir monolayer and the deposition methodology.

2. Langmuir-Blodgett methodology

The LB methodology consists on the transfer process from the air-water interface onto a solid substrate of a monomolecular layer of amphiphilic material adsorbed at the air-water interface [12]. The amphiphilic material is dissolved in a volatile solvent and dropped on the air-water interface. For optimal results, the solvent should have a positive spreading coefficient and be insoluble in the subphase [28]. After the spreading, the solvent evaporates and the material forms a monolayer. When the monolayer reaches the thermodynamic equilibrium, it is symmetrically compressed by using two barriers. The sequential isothermal compression changes the structure of the monomolecular film, which passes through a series of 2D states, referred to as gas, expanded and compressed liquids, and solid state. Consequently, knowing the 2D phase diagram of the film, it is possible to control its structure and associated physical and chemical properties. To transfer the film onto the solid, a flat substrate is immersed into the aqueous subphase and then extracted in a controlled way with the film adsorbed onto it, see **Figure 2a**. The transfer process can be repeated many times to obtain multilayers [12, 29] of different thickness and composition. During the transfer process, the surface pressure is maintained constant by barrier compression in order to compensate the loss of molecules transferred onto the solid. One variant of this methodology is the horizontal deposition technique, referred as Langmuir-Schaefer (LS) method. In the latter, the solid substrate is placed parallel to the air-water interface and deposition is done by contacting the substrate horizontally with the floating monolayer, see **Figure 2b**.

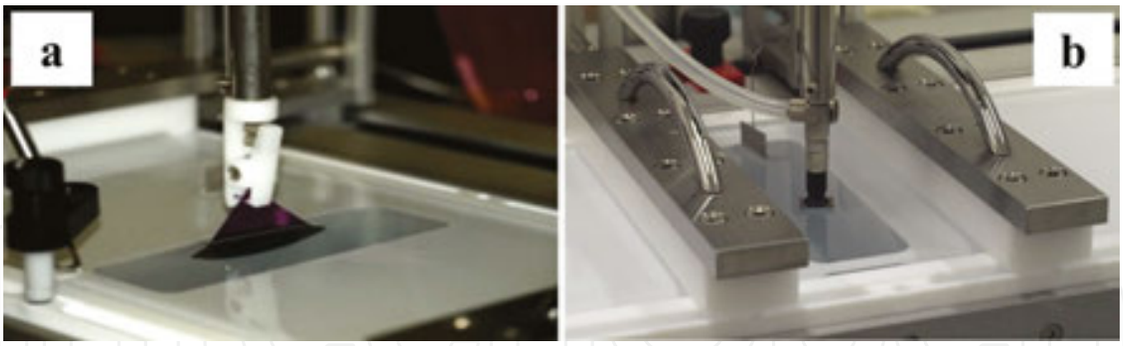

Figure 2. Langmuir-Blodgett (a) and Langmuir-Schaefer (b) transfer processes.

When the monolayer is transferred, its structure is often modified; therefore, to construct high-quality films, a careful control of experimental parameters, such as stability and homogeneity of the monolayer, subphase properties (composition, pH, presence of electrolytes, and temperature), substrate nature, speed of immersion/emersion of substrate, surface pressure during the deposition process, and the number of transferred monolayers, is required [12, 29].

3. The Langmuir-Blodgett films of graphene oxide derivatives

As commented previously, due to its unique properties graphene has been suggested to be used in a great number of technological applications. Nevertheless, each application requires a different set of properties. Thus, graphene synthesized by chemical vapor deposition (CVD) or micromechanical exfoliation renders high-quality sheets suitable for electronic applications; however, these sheets cannot be used for the fabrication of composites or water-soluble materials, because they do not contain functionalized groups. In these situations, graphene oxides [30] are preferred because they contain reactive oxygen functional groups that can attach small molecules, polymers, or nanoparticles to the graphitic surfaces for potential use in polymer composites [31], gas sensors [32], or photovoltaic cells [33, 34].

Another important issue of the use of graphene in technological applications is related to its implementation in devices. In the particular case of graphene oxide derivatives, conventional deposition techniques such as drop casting [9] or spin coating [10] not only induce aggregation of flakes, as can be seen in **Figure 1**, but also force the sheets to fold and wrinkle, losing its excellent properties [2]. Therefore, to overcome these limitations other deposition techniques such as LB have been recently proposed [16, 35].

Graphene oxide can be considered as an amphiphilic material [36] because it is constituted by two different domains. The hydrophobic one corresponds to π-conjugated sp^2 carbon while the hydrophilic domain is constituted by O-groups attached at the basal plane [37]. The existence of two regions allows obtaining stable water-insoluble monolayers of the material. Accordingly, several properties such as rheological properties, morphology, and stability of GO monolayers have been recently reported [11, 16, 18, 19]. Several works seem to indicate a great influence of the chemical composition on the film properties [19, 38].

http://dx.doi.org/10.5772/63495

Concerning the chemical synthesis, graphene oxide is usually obtained by graphite oxidation [17, 19, 39] or carbon nanofibers [18–20, 40] by means of the Staudenmaier [41] or the Hummers [42] reactions. Then, graphene oxides are often reduced by chemical agents [17, 43, 44] or thermal annealing [45, 46] to restore the graphene structure. However, both the GO reduced by chemical agents, referred as reduced graphene oxide (RGO), and the thermally reduced retain some O-groups attached to the basal plane of GO. These O-groups decrease the amazing properties of graphene such as transparency and high electric conductivity.

Despite the interest raised by GO, the knowledge of its chemical structure remains still a challenge. The best-known graphene oxide structure consists of two different carbon domains constituted by Csp^2 corresponding to aromatic groups and Csp^3 of alcohol and epoxy groups attached at the basal plane. The carboxylic acid groups are located at the edge of the sheets [37]. However, the main origin of the controversy is the percentage of each group into the flakes. Several are the causes of discrepancies, although the variability of the starting material and the oxidation process seem to be the most important ones [47]. On the other hand, the chemical structure of graphene oxide was recently revisited because it has been proved that the oxidation of carbon-based materials originates highly oxidized fragment, named as oxidative debris (OD) [47–49]. The oxidized fragments remain strongly adsorbed onto the graphitic sheets due to π-π staking interactions but can be removed by alkaline washing of graphene oxide. The purified GO contains lower O/C ratio than the non-purified one, and consequently its chemical structure and solubility properties are quite different [47, 49].

It is necessary to consider that in nanocomposites built with GO, the second component, polymers, nanoparticles, or small molecules, often interacts with the O-groups of graphene oxide; therefore, to improve the quality of the composite, it is crucial to have knowledge of the chemical structure of graphene oxide to control interactions between components which have a great influence on the properties of nanocomposites. However, there is no systematic study related to the effect of the oxidation procedure, nature of the starting material, and purification process on the chemical structure and properties of graphene oxides. Recently, we have started the systematic study of the effect of the starting material, reduction protocol, and purification process on the chemical structure of graphene oxides and on the film morphology. With this objective in mind, we have synthesized graphene oxides using graphite, and GANF® nanofibers from the Grupo Antolín Ingenieria (Burgos, Spain) as starting materials. The oxidation procedure was Hummer's reaction modified to obtain more oxidized samples [17, 18–20]. As reducing agents, we used hydrazine, vitamin C, and sodium borohydride. The purification process consisted of alkaline washing of graphene oxide and is previously reported [48, 49].

To quantify the oxidation degree of different materials, X-ray photoelectron spectroscopy (XPS) was employed. In all samples, the C1s core-level spectrum is an asymmetric band that can be fitted to three components centered at 284.8, 286.4, and 287.9 eV. These peaks are assigned to C-C bonds of the aromatic network, C-O bonds of alcohol or epoxide groups, and COOH groups, respectively [50]. From the area of these peaks, the percentage of the different groups in each sample was calculated. Results obtained for different kinds of graphene oxides are collected in **Figure 3**. Data shown in **Figure 3** were taken from references [17–19].

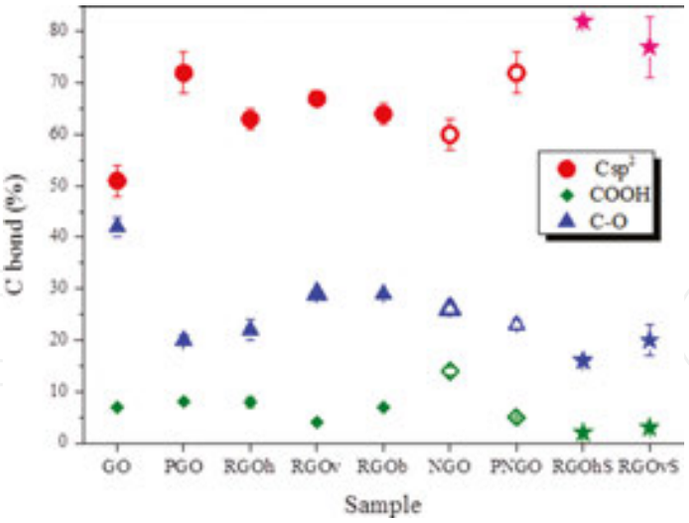

Figure 3. Chemical composition of graphene oxides determined by XPS measurements. Data were taken from references [17–19]. Solid symbols correspond to graphene oxides obtained from graphite and open symbols from GANF® nanofibers. Stars are results of surfactant-functionalized graphene oxides.

Results in **Figure 3** clearly show differences between the chemical composition of graphene oxides synthesized by the oxidation of graphite (GO) and nanofibers (NGO). Thus, the percentage of Csp^2 is slightly higher for NGO than for GO, while the percentage of C-O groups at the basal plane is higher for GO than for NGO and the percentage of COOH groups attached to NGO is twice that of GO. This behavior was attributed to the different size of nanoplatelets [18, 19]. In the case of NGO, dynamic light-scattering measurements (DLS) and the statistical analysis of FESEM images demonstrated that nanoplatelets of NGO are smaller than the GO ones; therefore, since the carboxylic groups are mainly localized at the edge of sheets the smallest sheets contain the highest proportions of COO^- groups [19]. As far as the influence of the purification procedure on the chemical composition, our results indicated that the percentage of Csp^2 increases after the alkaline washing. Moreover, the purification process drives to graphene oxides of similar chemical composition although the chemical structure of non-purified graphene oxides is quite different.

Another interesting result is that the percentage of Csp^2 of reduced graphene oxide is almost independent on the reducing agent, and the averaged value of 65 ± 2 is lower than the value found for purified graphene oxide, 72 ± 4. This fact was previously reported for graphene oxide reduced by hydrazine [47] and was interpreted as follows: due to the basic nature of hydrazine, it cleans oxidative debris and simultaneously reduces the oxygen groups of graphene oxide; however, nitrogen atoms remain attached to RGO sheets decreasing the percentage of Csp^2. This C-N bond identified by XPS as a peak centered at 400 eV is responsible for the increase of Csp^3 percentage. The balance of these processes leads to RGO sheets of intermediate composition between purified PGO and GO [17]. Similar situations were observed for graphene oxides reduced by vitamin C and borohydride, respectively. In these cases, oxygen and boron atoms of the oxidized product of vitamin C and borohydride remain attached to the network decreasing the aromatic degree of graphene derivatives. According to our results,

http://dx.doi.org/10.5772/63495

we postulate that alkaline washing must be the preferred procedure to increase the Csp^2 percentage on graphene oxide nanoplatelets.

Graphene oxide nanoplatelets are insulators and to increase the electric conductivity chemical reduction has been postulated. However, RGO films prepared by conventional deposition methodologies present low electrical conductivity values. This is probably due to the platelet aggregation induced by dewetting processes. We have explored the Langmuir-Blodgett methodology to obtain non-aggregated and ordered reduced graphene oxide films. To prepare the LB film, it is necessary to select the proper surface state, which will be transferred. To identify the surface state of materials at the interface, the compressional modulus, ε, has been widely used. The parameter can be calculated from the surface-pressure isotherm using Eq. (1):

$$\varepsilon = -A\left(\frac{\delta\Pi}{\delta A}\right)_{T,P} \tag{1}$$

In Eq. (1), A represents the surface area and π the surface pressure value. We have recorded the surface pressure isotherms of each material and a representative example is plotted in **Figure 4a**. The compressional elastic modulus value is plotted against the surface pressure in **Figure 4b**.

The isotherm morphology is similar to that of surfactant molecules and can be interpreted as follows: monolayers of surface pressure close to zero correspond to low values of compres-

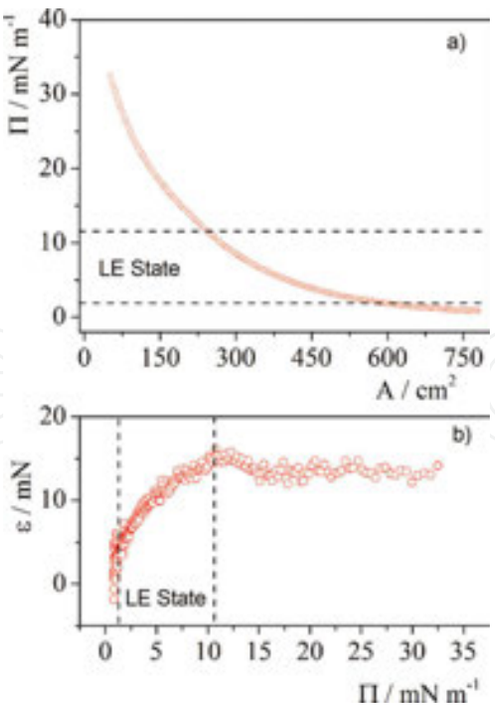

Figure 4. (a) Surface pressure and (b) compressional elastic modulus isotherms of graphene oxide reduced by borohydride at 293 K.

sional modulus and were assigned to surface states in which the nanoplatelets are isolated in a two-dimensional gas state. When the surface area decreases, the nanoplatelets are pushed closer to each other, resulting in small domains in which ε grows until it reaches a maximum value. This two-dimensional region is commonly assigned to the liquid-expanded (LE) state and corresponds to close-packed sheets. Beyond the compressional elastic modulus maximum, the nanoplatelets form wrinkles, overlaps, and three-dimensional (3D) structures [16].

In a previous work, the LE state of the GO monolayer [38] has been modeled by Volmer's model adapted to nanoparticles [51]. We have used this model to interpret the isotherms of different nanoplatelets of GO at the LE state. Our results demonstrated strong interactions between carboxylic acids at the edge of sheets through hydrogen bonds [18, 19].

Because we are interested to build GO films of closely packed and nonoverlapped nanoplatelets, we transferred graphene oxide monolayers at the LE state by the LB methodology [18, 19]. Representative atomic force microscopy (AFM) and FESEM images of these films are collected in **Figure 5**.

As can be seen in **Figure 5**, the solid coverage is higher for GO, **Figure 5a**, than for reduced graphene oxides, **Figure 5b**. Low coverage was also reported for purified graphene oxides [18,

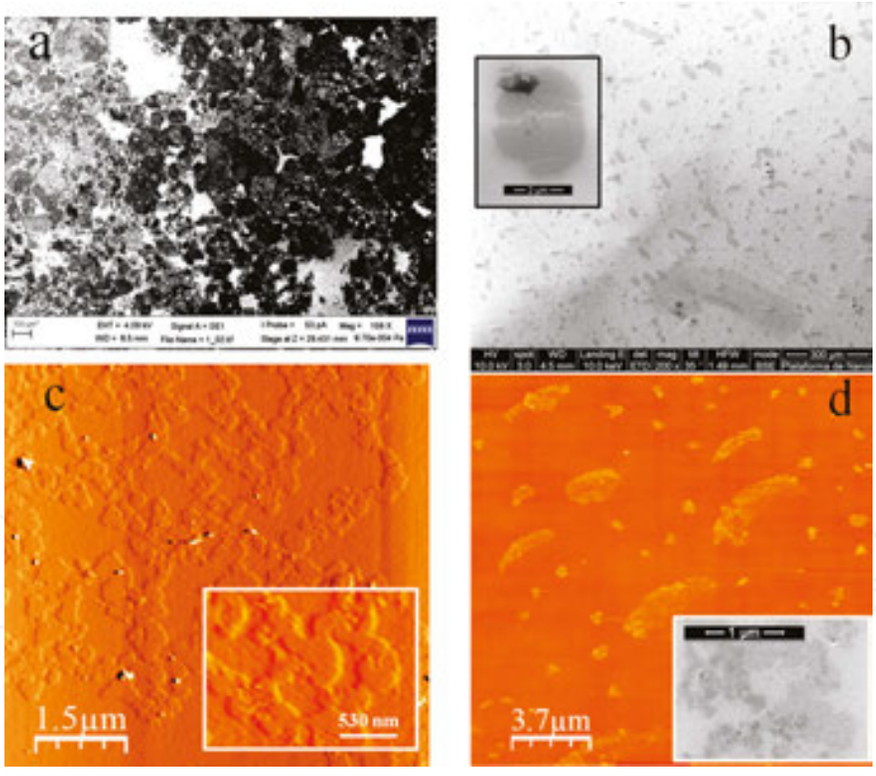

Figure 5. Representative images of different graphene oxides films: (a) SEM image of graphene oxide obtained by oxidation of graphite; (b) TEM image of graphene oxide reduced by vitamin C. The inset is a magnification to show the morphology of RGOv nanoplatelets; (c) graphene oxide functionalized with DDPS and reduced by hydrazine. The inset shows a magnification of the AFM image; (d) graphene oxide functionalized with DDPS and reduced by vitamin C. The inset is a TEM image to show details of the film morphology. Reduced graphene oxides were obtained using graphite as starting materials. The surface pressure of the Langmuir monolayer precursor of the LB film was 1 mN m^{-1}.

19] and was attributed to the low percentage of O-groups attached to sheets of purified oxides [19]. A high percentage of O-groups favor the contact between silanol groups of the silicon wafer and sheets increasing the adhesion of nanoplatelets to silicon. Since the chemical composition of reduced and purified graphene oxides is almost the same, the low percentage of O-groups at reduced samples can be responsible for the low coverage observed for RGO films.

In an attempt to improve the solid coverage, the reduced graphene oxides were functionalized with the zwitterionic surfactant N dodecyl-N,N-dimethyl-3-ammonio-1-propanesulfonate (DDPS). We have proved that the surfactant remains adsorbed onto graphene oxide platelets playing two important roles: as surface active molecule, it favours attractive interactions between the silicon and the reduced graphene oxide and because it is attached at sheets minimizing the restacking of flakes. It is interesting to note that the surfactant is attached to sheets in a non-covalent way, and consequently the chemical structure of graphene oxide is not significantly altered [52].

The AFM images of functionalized reduced graphene oxide films, **Figure 5c** and **d**, show that the functionalization with the DDPS surfactant increases the solid coverage; however, it is lower than that for graphene oxide, **Figure 5a**. The AFM images of RGOhS, **Figure 5c**, also show the formation of the chained sheets suggesting lateral attractive interactions between flakes. These attractive interactions can be likely induced by the surfactant molecules attached to the sheets [17].

We have great interest to study the effect of GO chemical composition on the electrical conductivity of GO films. However, in the case of reduced graphene oxide the electrical conductivity value is too small to detect significant differences; therefore, we employed an alternative method widely used by other authors. The method consists of measuring the conductivity of paper-like graphene oxide films [53]. To analyze the electrical conductivity dependence with the chemical composition, we have plotted the electrical conductivity against the Csp^2 and C-O group percentages shown in **Figure 6a** and **b**, respectively.

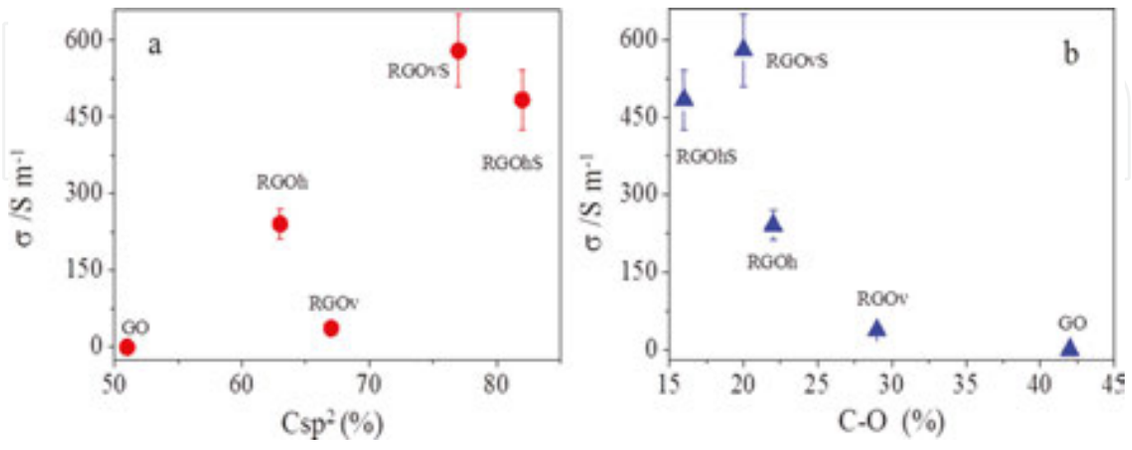

Figure 6. Variation of the electrical conductivity values of paper-like graphene oxide films with the Csp^2 (a) and (b) C-O group percentages, respectively. Data were taken from Reference [16].

Results in **Figure 6a** show that the electrical conductivity increases as the Csp^2 percentage. Moreover, the highest conductivity value is obtained for graphene oxide functionalized with the zwitterionic surfactant. In addition, samples with the lowest percentage of C-O and COOH groups, see **Figure 3**, correspond with reduced graphene oxides functionalized with the surfactant DDPS. All these facts suggest that the surfactant molecules can eliminate high amount of O-groups of samples increasing the electrical conductivity of flakes as can be seen in **Figure 6b**.

On summarizing, the LB technique can be presented as a good methodology of building graphene oxide films because it renders high-coverage and ordered films. On the other hand, the conductivity of our surfactant-functionalized RGO samples is higher than the values found in the literature for paper-like films of reduced graphene oxide [5, 54] functionalized with ionic surfactants, although more efforts must be done to improve the solid coverage and to increase the electrical conductivity values of graphene oxide films.

4. The Langmuir-Blodgett films of 2D materials: QDs and nanowires

Nanoparticles of CdSe Quantum Dots are semiconductors which show size dependence in their optoelectronic properties with attractive applications in the fabrication of solar cells or light-emitting diodes (LEDs) due to their band-gap tunability.

The most important optical advantages are a broad and continuous absorbance spectrum and a narrow emission spectrum whose maximum position and dynamic emission properties depend on its QD size. However, optoelectronic device applications based on nanoparticles require QDs assembly in controllable architecture to avoid the deterioration of the quantum film efficiency. Therefore, the thickness and uniformity of the assembled QD films are crucial factors in the emission properties of films [7, 55–58].

In the particular case of CdSe QDs, the hydrophobic nanoparticles present the highest quantum efficiency. However, when these nanoparticles are transferred from the air-water interface onto substrates such as glass, silicon, or mica without treatment to become the solid surface, hydrophobic, low coverage and nanoparticle agglomeration have been observed [59, 60]. These undesirable results decrease the quantum yield of nanoparticle films. To solve this problem, some approaches have been proposed. One of the most widely used strategies consists of mixing nanoparticles with surfactants or polymers and then transferring the mixture from the air-water interface onto the solid substrate [61–63]. This approach seeks to control the assembly of hydrophobic nanoparticles at the air-water interface. With this purpose, we have proposed three amphiphilic molecules of distinct nature, the copolymers poly(octadecene-co-maleic anhydride), PMAO, and poly(styrene-co-maleic anhydride) partial 2-butoxyethyl ester cumene terminated, PS-MA-BEE, and the Gemini surfactant ethyl-bis(dimethyl octadecylammonium bromide), 18-2-18. All these molecules present surface activity and can anchor to substrates such as mica, glass, or silicon, through their hydrophilic moieties [13, 14] favoring the QDs' adhesion across its hydrophobic part. We have chosen the polymer PMAO because it interacts effectively with hydrophobic nanoparticles leading to excellent stability by

http://dx.doi.org/10.5772/63495

avoiding 3D aggregation [64, 65]. In the case of the polymer PS-MA-BEE, it was chosen because it is a good component to organize hybrid nanomaterials used in submicrometric electronic devices [66]. This is due to its mechanical rigidity and good adhesion on solids [67]. Finally, the Gemini surfactant was chosen since it has been proposed in combination with DNA for biotechnological applications [68, 69].

Our results demonstrated that the QD aggregation is avoided by the addition of these polymer and surfactant molecules. Attractive interactions between the chains of these molecules and the hydrophobic moieties of the QD stabilizer, trioctylphosphine oxide (TOPO), favor the adsorption of QDs on the matrices, while the hydrophilic groups of polymer or surfactant molecules increase the QDs' adhesion in solid substrates, avoiding the nanoparticle agglomeration.

We also found two different film features depending on the film composition. To illustrate this behavior, **Figure 7** collects some AFM, transmission electron microscopy (TEM), and scanning electron microscopy (SEM) images of QD films prepared with different matrix compositions.

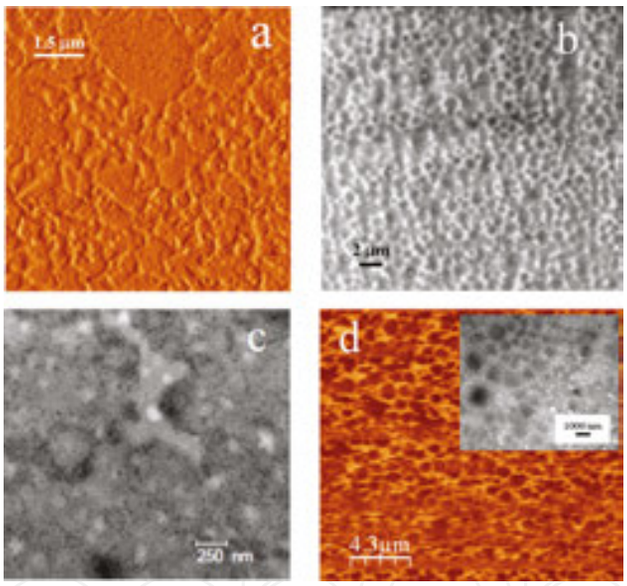

Figure 7. (a) AFM image of a Gemini/QD film at the surfactant mole fraction of 0.98, (b) SEM image of a PMAO/QD LB film onto mica at the polymer mole fraction of 0.50. The Langmuir monolayers were transferred at the surface pressure of 30 mN m^{-1}, (c) TEM image of mixed PS-MA-BEE/QD LB film of polymer mole fraction of 0.5 and deposited at the surface pressure of 14 mN m^{-1}, and (d) AFM image of a mixed PS-MA-BEE/QD film of polymer mole fraction of 0.96 and deposited at the surface pressure of 30 mN m^{-1}. The inset corresponds to the TEM image of the film.

Images in **Figure 7** show two different morphologies, hexagonal networks and domains of different shapes, depending on the film composition. Thus, mixed films of QDs and PS-MA-BEE of high polymer mole fraction, $X_P \geq 0.95$, and deposited at 30 mN m^{-1} [22] and PMAO/QDs films are constituted by hexagonal networks [21], **Figure 7b** and **d**. It is interesting to note that the height of rims around the holes was 4 nm, which is compatible with the diameter of the nanoparticles dissolved in chloroform (3.4 nm). This result indicates that QDs are mainly confined in rims and do not form 3D aggregates. On the other hand, all the Gemini/

QDs films and PS-MA-BEE/QDs films of polymer mole fraction below 0.95 deposited at low-surface pressure (14 mN m^{-1}) are constituted by domains of different morphologies, **Figure 7a** and **c**. The domain height determined by AFM measurements (~3 nm) is consistent with the diameter of QDs dissolved in chloroform. This fact indicates that there is no 3D aggregation in these films.

Differences between film morphologies were interpreted according to dewetting mechanisms [21, 22]. The two dewetting mechanisms considered in these cases are known as nucleation, growth, and coalescence of holes [70] and spinodal [71]. In the former, the gravity contribution predominates and the dewetting process starts with the nucleation of holes at film-defect sites followed by the material displacement away from the nucleus. The material is accumulated in the rims of holes delimiting a mosaic [70]. Conversely, in the spinodal dewetting mechanism, the capillary waves break the film into nanostructures when the amplitude of the capillary waves exceeds the thickness of the film. Taking into account that the molecular weight of the polymer PMAO is around 50 times higher than the surfactant one, it becomes clear that the gravitational effect prevailed over the capillary waves even in films with small amount of the polymer PMAO. Therefore, the PMAO/QDs film morphology is driven by the mechanism of nucleation, growth, and coalescence of holes, while spinodal dewetting mechanism prevails in Gemini/QD films [21]. In the case of PS-MA-BEE/QD films, the interpretation of the behavior observed is not so evident and it is necessary to analyze the balance between the driving forces involved in the surface arrangement: gravitational and capillary forces. Thus, the elasticity values go through a minimum for PS-MA-BEE/QDs monolayers at the surface pressure of 30 mN m^{-1} and for polymer mole ratio above 0.95, while it reaches maximum values for monolayers at the surface pressure value of 14 mN m^{-1} and $X_P < 0.95$ [22]. Taking into account that the damping coefficient passes through a maximum at low elasticity values and decreases when the elasticity modulus increases [22], it is easy to understand that in PS-MA-BEE/QD films of low elasticity values (π = 30 mN m^{-1} and $X_P \geq 0.95$), the capillary waves are quickly damped and the film breaks in domains separated by holes due to gravitational effects. Conversely, the capillary waves for monolayers with the highest elasticity values (π = 14 mN m^{-1} and $X_P < 0.95$) do not damp so quickly and they drive the dewetting mechanism. In these situations, the spinodal dewetting mechanism predominates against the growth of holes process leading to QD domains of different shapes [22].

Another interesting example is the preparation of silver nanowire films for manufacturing modern devices such as photovoltaic cells, touch panels, and light-emitting diodes. Although the development of new materials is mainly by the requirements of each application [72], high transparency and electrical conductivity always constitute required requisites.

Indium tin oxide (ITO) currently dominates the field of transparent conductive electrodes as a result of its excellent optoelectronic properties [73]; however, it suffers important limitations due to the scarcity of indium, brittleness of its electrodes, and high manufacturing cost. Several materials such as carbon nanotubes [74, 75], graphene films [76, 77], conducting polymers, and metal nanowires [72, 78] are being analyzed to replace ITO. However, the properties of these materials, in terms of electrical resistance and transparency, are still inferior to ITO [78]. Among all, the silver nanowires arouse great interest due to the high conductivity of silver (6.3×10^7 S

m^{-1}) [79]. Since the nanowires are usually synthesized in solution, an important issue is the control of the transfer process from solutions onto the substrate. This is because to achieve low electrical resistance and high transparency, it is necessary to optimize the morphology, the placement of nanowires, and the junction resistance between them in the network. As commented previously, spin-coating and drop-casting methodologies present several disadvantages since water evaporation leaves discontinuous films with typical coffee rings that significantly decrease the quality of AgNW films [80, 81]. To overcome these limitations, we have reported a strategy based on the Langmuir-Schaefer methodology to transfer hydrophobic AgNW from the air-water interface onto Lexan polycarbonate substrate in an ordered and controlled way [27].

The first step for building LB films is to obtain stable monolayers of hydrophobic materials. Therefore, it is necessary to synthesize hydrophobic nanowires, since the commercial ones are water soluble since they use polyvinyl pyrrolidone molecules as capping agents. To synthesize hydrophobic AgNW, polyvinyl pyrrolidone was replaced by octyl thiol molecules. The surface modification is achieved through the surface ligand exchange procedure reported by Tao [82]. After the synthesis of AgNW, they were deposited at the air-water interface and different surface states were transferred onto the solid substrate by the LS methodology. The surface states of nanowire monolayers are characterized by the surface compressional modulus, ε, calculated from the surface pressure isotherm and Eq. (1), and ε-values are plotted against the surface concentration, Γ, in **Figure 8a**. As can be seen in **Figure 8a**, when the surface concentration is small, the elasticity modulus value is close to zero. In this region, named as low-surface density state (LD), nanowires are randomly orientated. When the surface density is further increased and ε reaches a value of 10 mN m^{-1}, the monolayer is highly packed; we referred to this state as the high-surface density state (HD) [83].

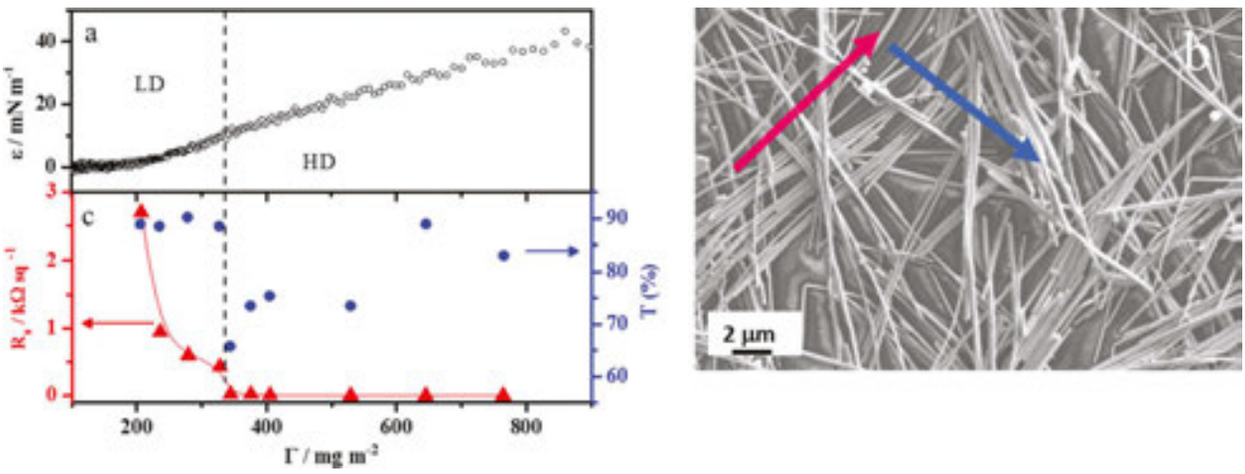

Figure 8. (a) Elasticity isotherm of silver nanowires capped with octyl thiol at 20°C, (b) FESEM image of a bilayer of AgNW of 645 mg m^{-2}. Arrows indicate the orientation of the first (red) and second (blue) layers, and (c) variation of sheet resistance and transmittance with the nanowire surface concentration of LS films.

We have transferred AgNW Langmuir monolayers at LD and HD states by the Langmuir-Schaefer methodology. With the purpose of achieving a network of nanowires, a second layer

in which the nanowires are oriented perpendicular to the first layer was deposited. In the first and second layers, the surface density of the transferred Langmuir monolayer was the same [27]. The surface density is controlled by the surface pressure value. **Figure 8b** shows a representative FE-SEM image of a nanowire film obtained by this methodology.

The sheet resistance, R_s, measured in Ω sq^{-1} and the transmittance measured at 550 nm are plotted against the surface concentration in **Figure 8c**. Data in **Figure 8c** show that the monolayers at the LD state present high R_s values which decrease when the surface concentration increases, while the transmittance value is almost independent on surface concentration and remains constant at 88%. The behavior is opposite for films built from Langmuir monolayers at the HD state. In this case, the sheet resistance is maintained at 8 Ω sq^{-1} while the transmittance value changes from 65 to 89% when the surface concentration was modified between 345 to 770 mg m^{-2}. According to the resistance and transparency values, our AgNW films can be employed as substitutes for ITO as components of devices such as touch screens, electromagnetic shielding, and defrosted windows [27]. Moreover, our results proved that the Langmuir-Schaefer methodology is a versatile technique, which allows modifying the transmittance keeping the sheet resistance or tuning the sheet resistance, maintaining the transparency of films constant by properly selecting the surface state and the nanowire mass transferred onto the solid substrate.

Results analyzed in this chapter allow us to discuss the ability of the Langmuir-Blodgett and Langmuir-Schaefer methodologies to build thin films of 2D materials such as graphene oxides, transition metal chalcogenide nanoparticles, CdSe Quantum Dots, and silver nanowires. We discuss the advantages of these methods against the most conventional ones such as drop and spin coating for built-in 2D material films with applications in the fabrication of solar cells, LEDs, sensors, and transparent electrodes.

We also review some strategies for improving the solid coverage, avoiding the nanoparticle aggregation, and modulating the film morphology. All these issues are crucial for increasing the quality of films and to modulate its properties according to the properties required for each application.

Results analyzed in this chapter indicate that the Langmuir-Blodgett and Langmuir-Schaefer methodologies combined with self-assembled materials can be proposed as a non-template reproducible technique for patterning at the nanoscale. However, most efforts have to be done for achieving more homogeneous films, higher coverage, and a greater control of the material arrangements to build good-quality films to be used in technological applications.

Acknowledgements

The authors thank financial support from the European Regional Development Fund, ERDF, Ministerio de Educación y Ciencia (MAT 2010-19727), and Ministerio de Economía y Competitividad (IPT-2012-0429-420000). TA and BMG wish to thank the European Social Fund and Consejería de Educación de la Junta de Castilla y León for their FPI grants. We also thank Ultra-

Intense Lasers Pulsed Center of Salamanca (CLPU) for the AFM measurements, to Microscopy Service (Universidad de Salamanca) for the TEM measurements, and Sala Blanca de Nanotecnología (USAL) for FE-SEM facility. We thank Dr. García Fierro (Instituto de Catálisis y Petroleoquímica, Madrid) for XPS measurements.

Author details

María Mercedes Velázquez*, Teresa Alejo, David López-Díaz, Beatriz Martín-García and María Dolores Merchán

*Address all correspondence to: mvsal@usal.es

Department of Physical Chemistry, Faculty of Chemistry, University of Salamanca, Salamanca, Spain

References

[1] Novoselov K S, Geim A K, Morozov S V, Jiang D, Zhang Y, Dubonos S V, Grigorieva I V, Firsov A A. Electric Field Effect in Atomically Thin Carbon Films. Science. 2004; 306: 666–669. DOI: 10.1126/science.1102896

[2] Geim A K, Novoselov K S. The Rise of Graphene. Nature Materials. 2007; 6: 183–191. DOI: 10.1038/nmat1849

[3] Geim A K. Graphene: Status and Prospects. Science. 2009; 324: 1530–1534. DOI: 10.1126/science.1158877

[4] Castro Neto A H, Guinea F, Peres N M R, Novoselov K S, Geim A K. The Electronic Properties of Graphene. Reviews of Modern Physics. 2009; 81: 109–162.

[5] Lotya M, Hernandez Y, King P J, Smith R J, Nicolosi V, Karlsson L S, Blighe F M, De S, Wang Z, McGovern I T, Duesberg G S, Coleman J N. Liquid Phase Production of Graphene by Exfoliation of Graphite in Surfactant/Water Solutions. Journal of the American Chemical Society. 2009; 131: 3611–3620. DOI: 10.1021/ja807449u

[6] Park S, Ruoff R S. Chemical Methods for the Production of Graphenes. Nature Nanotechnology. 2009; 4: 217–224. DOI: 10.1038/nnano.2009.58

[7] Talapin D V, Lee J-S, Kovalenko M V, Shevchenko E V. Prospects of Colloidal Nanocrystals for Electronic and Optoelectronic Applications. Chemical Reviews. 2010; 110: 389–458. DOI: 10.1021/cr900137k

[8] Wang J, Vennerberg D, Lin Z. Quantum Dot Sensitized Solar Cells. Journal of Nanoengineering and Nanomanufacturing. 2011; 1: 155–171. DOI: 10.1166/jnan.2011.1057

[9] Gilje S, Han S, Wang M, Wang K L, Kaner R B. A Chemical Route to Graphene for Device Applications. Nano Letters. 2007; 7: 3394–3398. DOI: 10.1021/nl0717715

[10] Becerril H A, Mao J, Liu Z, Stoltenberg R M, Bao Z, Chen Y. Evaluation of Solution-Processed Reduced Graphene Oxide Films as Transparent Conductors. ACS Nano. 2008; 2: 463–470. DOI: 10.1021/nn700375n

[11] Zheng Q, Li Z, Yang J, Kim J-K. Graphene Oxide-based Transparent Conductive Films. Progress in Materials Science. 2014; 64: 200–247. DOI: 10.1016/j.pmatsci.2014.03.004

[12] Roberts G G. Langmuir-Blodgett Films. New York: Springer US; 1990. 425 p. DOI: 10.1007/978-1-4899-3716-2

[13] Martín-García B, Velázquez M M, Pérez-Hernandez J A, Hernandez-Toro J. Langmuir and Langmuir-Blodgett Films of a Maleic Anhydride Derivative: Effect of Subphase Divalent Cations. Langmuir. 2010; 26: 14556–14562. DOI: 10.1021/la101736e

[14] Alejo T, Merchán M D, Velázquez M M. Specific Ion Effects on the Properties of Cationic Gemini Surfactant Monolayers. Thin Solid Films. 2011; 519: 5689–5695. DOI: 10.1016/j.tsf.2011.03.018

[15] Collier C P, Saykally R J, Shiang J J, Henrichs S E, Heath J R. Reversible Tuning of Silver Quantum Dot Monolayers Through the Metal-Insulator Transition. Science. 1997; 277: 1978–1981. DOI: 10.1126/science.277.5334.1978

[16] Cote L J, Kim F, Huang J. Langmuir-Blodgett Assembly of Graphite Oxide Single Layers. Journal of the American Chemical Society. 2008; 131: 1043–1049. DOI: 10.1021/ja806262m

[17] Martín-García B, Velázquez M M, Rossella F, Bellani V, Diez E, García Fierro J L, Pérez-Hernández J A, Hernández-Toro J, Claramunt S, Cirera A. Functionalization of Reduced Graphite Oxide Sheets with a Zwitterionic Surfactant. ChemPhysChem. 2012; 13: 3682–3690. DOI: 10.1002/cphc.201200501

[18] López-Díaz D, Mercedes Velázquez M, Blanco de La Torre S, Pérez-Pisonero A, Trujillano R, Fierro J L G, Claramunt S, Cirera A. The Role of Oxidative Debris on Graphene Oxide Films. ChemPhysChem. 2013; 14: 4002–4009. DOI: 10.1002/cphc.201300620

[19] Hidalgo R S, López-Díaz D, Velázquez M M. Graphene Oxide Thin Films: Influence of Chemical Structure and Deposition Methodology. Langmuir. 2015; 31: 2697–2705. DOI: 10.1021/la5029178

[20] Orna J, López-Díaz D, Pérez A, Rodríguez M J, Lagunas A R, Velázquez M M, Blanco S, Merino C. GRAnPH®: High Quality Graphene Oxide Obtained from GANF® Carbon Nanofibres. In: *eNanonewsletter*. Antonio Correia, Madrid, Spain: Phantoms Foundation; 2013. pp 33–37

[21] Alejo T, Merchán M D, Velázquez M M, Pérez-Hernández J A. Polymer/Surfactant Assisted Self-assembly of Nanoparticles into Langmuir–Blodgett Films. Materials Chemistry and Physics. 2013; 138: 286–294. DOI: 10.1016/j.matchemphys.2012.11.058

[22] Martín-García B, Velázquez M M. Block Copolymer Assisted Self-assembly of Nanoparticles into Langmuir-Blodgett Films: Effect of Polymer Concentration. Materials Chemistry and Physics. 2013; 141: 324–332. DOI: 10.1016/j.matchemphys.2013.05.017

[23] Martín-García B, Paulo P M R, Costa S M B, Velázquez M M. Photoluminescence Dynamics of CdSe QD/Polymer Langmuir-Blodgett Thin Films: Morphology Effects. The Journal of Physical Chemistry C. 2013; 117: 14787–14795. DOI: 10.1021/jp311492z

[24] Alejo T, Martín-García B, Merchán M D, Velázquez M M. QDs Supported on Langmuir-Blodgett Films of Polymers and Gemini Surfactant. Journal of Nanomaterials. 2013; 2013: 1–10. DOI: 10.1155/2013/287094

[25] Alejo T, Merchán M D, Velázquez M M. Adsorption of Quantum Dots onto Polymer and Gemini Surfactant Films: A Quartz Crystal Microbalance Study. Langmuir. 2014; 30: 9977–9984. DOI: 10.1021/la5024955

[26] Martín-García B, Velázquez M M. Nanoparticle Self-assembly Assisted by Polymers: The Role of Shear Stress in the Nanoparticle Arrangement of Langmuir and Langmuir–Blodgett Films. Langmuir. 2014; 30: 9977-9984. DOI: 10.1021/la404834b

[27] Lopez-Diaz D, Merino C, Velázquez M. Modulating the Optoelectronic Properties of Silver Nanowires Films: Effect of Capping Agent and Deposition Technique. Materials. 2015; 8: 5405. DOI: 10.3390/ma8115405

[28] Gaines G L J. Insoluble Monolayers at Liquid-Gas Interfaces. New York: Interscience; 1966.

[29] Petty M C. Langmuir-Blodgett Films: An Introduction. New York: Cambridge University Press; 1996. DOI: 10.1017/CBO9780511622519

[30] Zhu Y, Murali S, Cai W, Li X, Suk J W, Potts J R, Ruoff R S. Graphene and Graphene Oxide: Synthesis, Properties, and Applications. Advanced Materials. 2010; 22: 3906–3924. DOI: 10.1002/adma.201001068

[31] Potts J R, Dreyer D R, Bielawski C W, Ruoff R S. Graphene-Based Polymer Nanocomposites. Polymer. 2011; 52: 5–25. DOI: 10.1016/j.polymer.2010.11.042

[32] Prezioso S, Perrozzi F, Giancaterini L, Cantalini C, Treossi E, Palermo V, Nardone M, Santucci S, Ottaviano L. Graphene Oxide as a Practical Solution to High Sensitivity Gas Sensing. The Journal of Physical Chemistry C. 2013; 117: 10683–10690. DOI: 10.1021/jp3085759

[33] Eda G, Chhowalla M. Chemically Derived Graphene Oxide: Towards Large-Area Thin-Film Electronics and Optoelectronics. Advanced Materials. 2010; 22: 2392–2415. DOI: 10.1002/adma.200903689

[34] Loh K P, Bao Q, Eda G, Chhowalla M. Graphene oxide as a Chemically Tunable Platform for Optical Applications. Nature Chemistry. 2010; 2: 1015–1024.

[35] Zheng Q, Ip W H, Lin X, Yousefi N, Yeung K K, Li Z, Kim J-K. Transparent Conductive Films Consisting of Ultralarge Graphene Sheets Produced by Langmuir–Blodgett Assembly. ACS Nano. 2011; 5: 6039–6051. DOI: 10.1021/nn2018683

[36] Kim J, Cote L J, Huang J. Two Dimensional Soft Material: New Faces of Graphene Oxide. Accounts of Chemical Research. 2012; 45: 1356–1364. DOI: 10.1021/ar300047s

[37] Lerf A, He H, Forster M, Klinowski J. Structure of Graphite Oxide Revisited. The Journal of Physical Chemistry B. 1998; 102: 4477–4482. DOI: 10.1021/jp9731821

[38] Imperiali L, Liao K-H, Clasen C, Fransaer J, Macosko C W, Vermant J. Interfacial Rheology and Structure of Tiled Graphene Oxide Sheets. Langmuir. 2012; 28: 7990–8000. DOI: 10.1021/la300597n

[39] Dreyer D R, Park S, Bielawski C W, Ruoff R S. The Chemistry of Graphene Oxide. Chemical Society Reviews. 2010; 39: 228–240. DOI: 10.1039/b917103g

[40] Varela-Rizo H, Rodriguez-Pastor I, Merino C, Martin-Gullon I. Highly Crystalline Graphene Oxide Nano-Platelets Produced from Helical-Ribbon Carbon Nanofibers. Carbon. 2010; 48: 3640–3643. DOI: 10.1016/j.carbon.2010.05.033

[41] Staudenmaier L. Verfahren zur Darstellung der Graphitsäure. Methods for synthesizing graphite acid. 1898; 31: 1481–1487. DOI: 10.1002/cber.18980310237

[42] Hummers W S, Offeman R E. Preparation of Graphitic Oxide. Journal of the American Chemical Society. 1958; 80: 1339–1339. DOI: 10.1021/ja01539a017

[43] Stankovich S, Dikin D A, Piner R D, Kohlhaas K A, Kleinhammes A, Jia Y, Wu Y, Nguyen S T, Ruoff R S. Synthesis of Graphene-Based Nanosheets via Chemical Reduction of Exfoliated Graphite Oxide. Carbon. 2007; 45: 1558–1565. DOI: 10.1016/j.carbon.2007.02.034

[44] Fernández-Merino M J, Guardia L, Paredes J I, Villar-Rodil S, Solís-Fernández P, Martínez-Alonso A, Tascón J M D. Vitamin C Is an Ideal Substitute for Hydrazine in the Reduction of Graphene Oxide Suspensions. The Journal of Physical Chemistry C. 2010; 114: 6426–6432. DOI: 10.1021/jp100603h

[45] Bagri A, Mattevi C, Acik M, Chabal Y J, Chhowalla M, Shenoy V B. Structural Evolution During the Reduction of Chemically Derived Graphene Oxide. Nature Chemistry. 2010; 2: 581–587. DOI: 10.1038/nchem.686

[46] Claramunt S, Varea A, López-Díaz D, Velázquez M M, Cornet A, Cirera A. The Importance of Interbands on the Interpretation of the Raman Spectrum of Graphene Oxide. The Journal of Physical Chemistry C. 2015; 119: 10123–10129. DOI: 10.1021/acs.jpcc.5b01590

[47] Thomas H R, Day S P, Woodruff W E, Vallés C, Young R J, Kinloch I A, Morley G W, Hanna J V, Wilson N R, Rourke J P. Deoxygenation of Graphene Oxide: Reduction or Cleaning? Chemistry of Materials 2013; 25: 3580–3588 DOI: 10.1021/cm401922e

[48] Wang Z, Shirley M D, Meikle S T, Whitby R L D, Mikhalovsky S V. The Surface Acidity of Acid Oxidised Multi-Walled Carbon Nanotubes and the Influence of In-situ Generated Fulvic Acids on Their Stability in Aqueous Dispersions. Carbon. 2009; 47: 73–79. DOI: 10.1016/j.carbon.2008.09.038

[49] Rourke J P, Pandey P A, Moore J J, Bates M, Kinloch I A, Young R J, Wilson N R. The Real Graphene Oxide Revealed: Stripping the Oxidative Debris from the Graphene-like Sheets. Angewandte Chemie International Edition. 2011; 50: 3173–3177. DOI: 10.1002/anie.201007520

[50] Hontoria-Lucas C, López-Peinado A J, López-González J D D, Rojas-Cervantes M L, Martín-Aranda R M. Study of Oxygen-Containing Groups in a Series of Graphite Oxides: Physical and Chemical Characterization. Carbon. 1995; 33: 1585–1592. DOI: 10.1016/0008-6223(95)00120-3

[51] Fainerman V B, Kovalchuk V I, Lucassen-Reynders E H, Grigoriev D O, Ferri J K, Leser M E, Michel M, Miller R, Möhwald H. Surface-Pressure Isotherms of Monolayers Formed by Microsize and Nanosize Particles. Langmuir. 2006; 22: 1701–1705. DOI: 10.1021/la052407t

[52] Qi X, Pu K-Y, Li H, Zhou X, Wu S, Fan Q-L, Liu B, Boey F, Huang W, Zhang H. Amphiphilic Graphene Composites. Angewandte Chemie International Edition. 2010; 49: 9426–9429. DOI: 10.1002/anie.201004497

[53] Gao W, Alemany L B, Ci L, Ajayan P M. New Insights into the Structure and Reduction of Graphite Oxide. Nature Chemistry. 2009; 1: 403–408.

[54] Fernández-Merino MJ, Paredes J I, Villar-Rodil S, Guardia L, Solís-Fernández P, Salinas-Torres D, Cazorla-Amorós D, Morallón E, Martínez-Alonso A, Tascón JMD. Investigating the Influence of Surfactants on the Stabilization of Aqueous Reduced Graphene Oxide Dispersions and the Characteristics of Their Composite Films. Carbon. 2012; 50: 3184–3194. DOI: doi:10.1016/j.carbon.2011.10.039

[55] Rogach A L. Semiconductor Nanocrystal Quantum Dots: Synthesis, Assembly, Spectroscopy and Applications. New York: Springer-Verlag Wien; 2008. 372 p. DOI: 10.1007/978-3-211-75237-1

[56] Tomczak N, Jańczewski D, Han M, Vancso G J. Designer Polymer–Quantum Dot Architectures. Progress in Polymer Science. 2009; 34: 393–430. DOI: 10.1016/j.progpolymsci.2008.11.004

[57] Kim T-H, Cho K-S, Lee E K, Lee S J, Chae J, Kim J W, Kim D H, Kwon J-Y, Amaratunga G, Lee S Y, Choi B L, Kuk Y, Kim J M, Kim K. Full-Colour Quantum Dot Displays

Fabricated by Transfer Printing. Nature Photonics. 2011; 5: 176–182. DOI: 10.1038/nphoton.2011.12

[58] Selinsky R S, Ding Q, Faber M S, Wright J C, Jin S. Quantum Dot Nanoscale Heterostructures for Solar Energy Conversion. Chemical Society Reviews. 2013; 42: 2963–2985. DOI: 10.1039/C2CS35374A

[59] Lambert K, Capek R K, Bodnarchuk M I, Kovalenko M V, Van Thourhout D, Heiss W, Hens Z. Langmuir-Schaefer Deposition of Quantum Dot Multilayers. Langmuir. 2010; 26: 7732–7736. DOI: 10.1021/la904474h

[60] Dabbousi B O, Murray C B, Rubner M F, Bawendi M G. Langmuir-Blodgett Manipulation of Size-Selected CdSe Nanocrystallites. Chemistry of Materials. 1994; 6: 216–219. DOI: 10.1021/cm00038a020

[61] Gupta S, Singh N, Sastry M, Kakkar R, Pasricha R. Controlling the Assembly of Hydrophobized Gold Nanoparticles at the Air–Water Interface by Varying the Interfacial Tension. Thin Solid Films. 2010; 519: 1072–1077. DOI: 10.1016/j.tsf.2010.08.046

[62] Pohjalainen E, Pohjakallio M, Johans C, Kontturi K, Timonen J V, Ikkala O, Ras R H, Viitala T, Heino M T, Seppala E T. Cobalt Nanoparticle Langmuir-Schaefer Films on Ethylene Glycol Subphase. Langmuir. 2010; 26: 13937–13943. DOI: 10.1021/la101630q

[63] Gattas-Asfura K M, Constantine C A, Lynn M J, Thimann D A, Ji X, Leblanc R M. Characterization and 2D Self-Assembly of CdSe Quantum Dots at the Air-Water Interface. Journal of the American Chemical Society. 2005; 127: 14640–14646. DOI: 10.1021/ja0514848

[64] Shtykova E V, Huang X, Gao X, Dyke J C, Schmucker A L, Dragnea B, Remmes N, Baxter D V, Stein B, Konarev P V, Svergun D I, Bronstein L M. Hydrophilic Monodisperse Magnetic Nanoparticles Protected by an Amphiphilic Alternating Copolymer. The Journal of Physical Chemistry C. 2008; 112: 16809–16817. DOI: 10.1021/jp8053636

[65] Bronstein L M, Shtykova E V, Malyutin A, Dyke J C, Gunn E, Gao X, Stein B, Konarev P V, Dragnea B, Svergun D I. Hydrophilization of Magnetic Nanoparticles with Modified Alternating Copolymers. Part 1: The Influence of the Grafting. The Journal of Physical Chemistry C. 2010; 114: 21900–21907. DOI: 10.1021/jp107283w

[66] Jones R, Winter C S, Tredgold R H, Hodge P, Hoorfar A. Electron-Beam Resists from Langmuir-Blodgett Films of Poly(styrene/maleic anhydride) Derivatives. Polymer. 1987; 28: 1619–1626. DOI: 10.1016/0032-3861(87)90001-2

[67] John Collins S, L. Mary N, Radhakrishnan G, Dhathathreyan A. Studies of Spread Monolayers of Derivative of Styrene-maleic Anhydride Copolymers. Journal of the Chemical Society, Faraday Transactions. 1997; 93: 4021–4023. DOI: 10.1039/A704115B

[68] Chen X, Wang J, Shen N, Luo Y, Li L, Liu M, Thomas R K. Gemini Surfactant/DNA Complex Monolayers at the Air-Water Interface: Effect of Surfactant Structure on the

Assembly, Stability, and Topography of Monolayers. Langmuir. 2002; 18: 6222–6228. DOI: 10.1021/la025600l

[69] Chen Q, Kang X, Li R, Du X, Shang Y, Liu H, Hu Y. Structure of the Complex Monolayer of Gemini Surfactant and DNA at the Air/Water Interface. Langmuir. 2012; 28: 3429–3438. DOI: 10.1021/la204089u

[70] Gentili D, Foschi G, Valle F, Cavallini M, Biscarini F. Applications of Dewetting in Micro and Nanotechnology. Chemical Society Reviews. 2012; 41: 4430–4443. DOI: 10.1039/c2cs35040h

[71] Reiter G. Dewetting of Thin Polymer Films. Physical Review Letters. 1992; 68: 75–78. DOI: 10.1103/PhysRevLett.68.75

[72] Langley D, Giusti G, Mayousse C, Celle C, Bellet D, Simonato J-P. Flexible Transparent Conductive Materials Based on Silver Nanowire Networks: A Review. Nanotechnology. 2013; 24: 452001. DOI: 10.1088/0957-4484/24/45/452001

[73] Alam M J, Cameron D C. Investigation of Annealing Effects on Sol–Gel Deposited Indium Tin Oxide Thin Films in Different Atmospheres. Thin Solid Films. 2002; 420–421: 76–82. DOI: 10.1016/S0040-6090(02)00737-X

[74] Wu Z, Chen Z, Du X, Logan J M, Sippel J, Nikolou M, Kamaras K, Reynolds J R, Tanner D B, Hebard A F, Rinzler A G. Transparent, Conductive Carbon Nanotube Films. Science. 2004; 305: 1273–1276. DOI: 10.1126/science.1101243

[75] Doherty E M, De S, Lyons P E, Shmeliov A, Nirmalraj P N, Scardaci V, Joimel J, Blau W J, Boland J J, Coleman J N. The Spatial Uniformity and Electromechanical Stability of Transparent, Conductive Films of Single Walled Nanotubes. Carbon. 2009; 47: 2466–2473. DOI: 10.1016/j.carbon.2009.04.040

[76] Moon I K, Kim J I, Lee H, Hur K, Kim W C, Lee H. 2D Graphene Oxide Nanosheets as an Adhesive Over-Coating Layer for Flexible Transparent Conductive Electrodes. Scientific Reports. 2013; 3: 1–7. DOI: 10.1038/srep01112

[77] Yun Y S, Kim D H, Kim B, Park H H, Jin H J. Transparent Conducting Films Based on Graphene Oxide/Silver Nanowire Hybrids with High Flexibility. Synthetic Metals. 2012; 162: 1364–1368. DOI: 10.1016/j.synthmet.2012.05.026

[78] Madaria A, Kumar A, Ishikawa F, Zhou C. Uniform, Highly Conductive, and Patterned Transparent Films of a Percolating Silver Nanowire Network on Rigid and Flexible Substrates Using a Dry Transfer Technique. Nano Research. 2010; 3: 564–573. DOI: 10.1007/s12274-010-0017-5

[79] Serway R A. Principles of Physics. 2nd Ed. Fort Worth, Texas: Saunder Colloge Pub.; 1998. p. 602.

[80] Deegan R D, Bakajin O, Dupont T F, Huber G, Nagel S R, Witten T A. Capillary Flow as the Cause of Ring Stains from Dried Liquid Drops. Nature. 1997; 389: 827–829. DOI: 10.1038/39827

[81] Huang J, Fan R, Connor S, Yang P. One-Step Patterning of Aligned Nanowire Arrays by Programmed Dip Coating. Angewandte Chemie International Edition. 2007; 46: 2414–2417. DOI: 10.1002/anie.200604789

[82] Tao A, Kim F, Hess C, Goldberger J, He R, Sun Y, Xia Y, Yang P. Langmuir-Blodgett Silver Nanowire Monolayers for Molecular Sensing Using Surface-Enhanced Raman Spectroscopy. Nano Letters. 2003; 3: 1229–1233. DOI: 10.1021/nl0344209

[83] Gonçalves da Silva A M, Romão R S, Lucero Caro A, Rodriguez Patino J M. Memory Effects on the Interfacial Characteristics of Dioctadecyldimethylammonium Bromide Monolayers at the Air–Water Interface. Journal of Colloid and Interface Science. 2004; 270: 417–425. DOI: 10.1016/j.jcis.2003.11.002

IntechOpen